Macromolecules

ARTICLE

pubs.acs.org/Macromolecules

Effect of Crystallization on the Electronic Energy Levels and Thin Film Morphology of P3HT:PCBM Blends

Wing C. Tsoi,[†,‡] Steve J. Spencer,[‡] Li Yang,[‡] Amy M. Ballantyne,[†] Patrick G. Nicholson,[‡] Alan Turnbull,[‡] Alex G. Shard,[‡] Craig E. Murphy,[*,‡] Donal D. C. Bradley,[†] Jenny Nelson,[†] and Ji-Seon Kim[*,†]

[†]Department of Physics and Centre for Plastic Electronics, Imperial College London, London SW7 2AZ, U.K.

[‡]National Physical Laboratory, Teddington, Middlesex TW11 0LW, U.K.

ABSTRACT: We study thin films of semi-crystalline regioregular poly(3-hexylthiophene) (RR-P3HT) and amorphous regiorandom P3HT (RRa-P3HT) in blends with [6,6]-phenyl C_{61} butyric acid methyl ester (PCBM). Ultraviolet and (angle-resolved) X-ray photoelectron spectroscopy techniques together with absorption, photoluminescence and optical microscopy were used to measure electronic energy levels, vertical chemical compositions and optical properties of these films. We find that ordering the P3HT chains raises the highest occupied molecular orbital (HOMO) energy level of P3HT thin films (reducing ionization potential) and that the ordering of P3HT chains occurs preferentially at the film−air interface in RR-P3HT:PCBM thin films. This leads to a vertical phase separation between P3HT and PCBM molecules, which may be undesirable for conventional P3HT:PCBM solar cells.

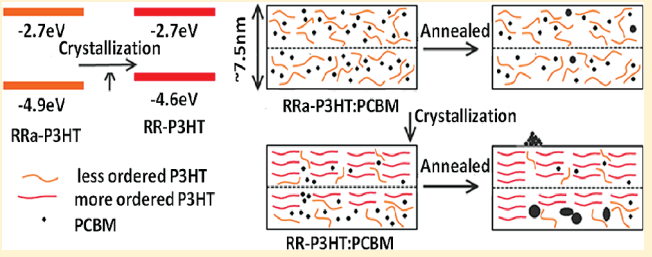

INTRODUCTION

Conjugated polymers are promising materials for low-cost solar cells as they can be solution-processed, thereby allowing coating and printing approaches to fabrication.[1,2] However, the power conversion efficiency of many conjugated polymer-based solar cells is relatively modest due to unoptimized optoelectronic properties.[1,3]

Regioregular poly(3-hexylthiophene) (RR-P3HT) blended with [6,6]-phenyl C_{61} butyric acid methyl ester (PCBM) has been intensely studied as the photoactive layer of a solar cell because it can reach a high power conversion efficiency of 4−5%.[4,5] Thermal or solvent annealing of the blend film is generally required to increase the efficiency further above 1−2%.[6−8] The dramatic increase of efficiency is mainly assigned to increased crystallization of RR-P3HT leading to improved hole mobility,[5,9] charge percolation pathways[8] and optical absorption.[5,9]

The blend film morphology of the components is crucial for charge separation/recombination and charge extraction.[10−12] Recently, by using variable-angle spectroscopic ellipsometry, Campoy-Quiles et al. showed that an unfavorable vertical phase separation can occur in blend films under certain circumstances leading to a significant fraction of RR-P3HT molecules (hole transporting material) at the film−air interface (where electron collecting electrode is subsequently deposited) and PCBM at the film−substrate interface.[6] This deduction is supported by X-ray photoelectron spectroscopy (XPS),[13] near-edge X-ray absorption fine structure[14] and neutron reflectivity measurements.[15,16] Such vertical phase separation have been also reported for other conjugated polymer: fullerene films.[17] On the other hand, cross-sectional transmission electron microscopy (TEM) images show column-like vertical structures with continuous pathways for RR-P3HT and PCBM respectively.[18] Electron tomography shows that after thermal annealing of RR-P3HT:PCBM blend film, there are favorable concentration of gradients of both RR-P3HT and PCBM through the thickness of the photoactive layer.[19]

The effects of the P3HT crystallization on its frontier electronic energy levels and the thin film morphology of P3HT:PCBM film near the surface remain, however, to be elucidated. The energies of highest occupied molecular orbital (HOMO) and lowest unoccupied molecular orbital (LUMO) are important for open circuit voltage (V_{oc}) and charge transfer between electron donor and electron acceptor. It has been argued that V_{oc} varies in proportion to the energy difference between the HOMO level of the donor and the LUMO level of the acceptor.[20]

In this paper, it is our motivation to study how the crystallization of P3HT affects its HOMO level and particularly the nature of thin film morphology nears the film−air interface, when blended with PCBM. We used a regiorandom poly(3-hexylthiophene) (RRa-P3HT), which is amorphous, as a reference material and compared it with a RR-P3HT which is semicrystalline. We also study blends of these polymers with PCBM before and after thermal annealing. Chlorobenzene was used as the solvent for the film preparation. Here, we used ultraviolet photoelectron spectroscopy (UPS) to study the solid-state HOMO energy levels of the films and angle-resolved X-ray photoelectron spectroscopy (AR-XPS) to study the thin film morphology near the film−air interface. Both UPS and XPS are highly surface sensitive techniques as the detected signal is

Received: December 14, 2010
Revised: February 15, 2011
Published: March 30, 2011

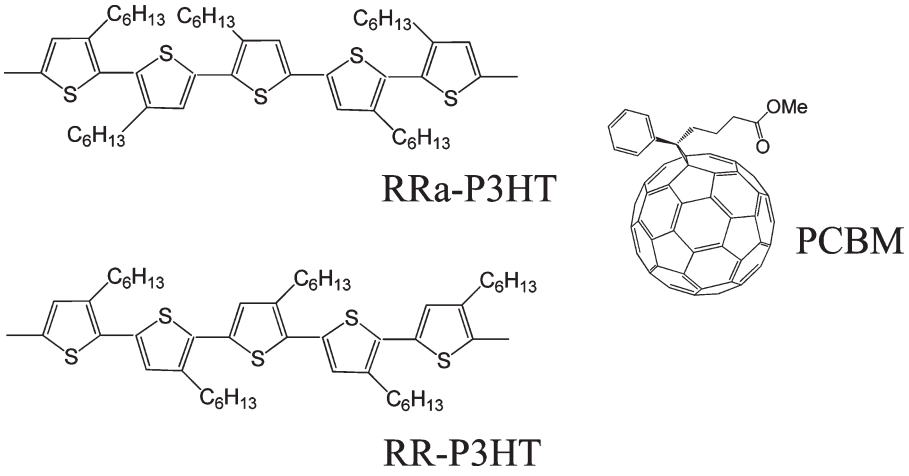

Figure 1. Molecular structure of RRa-P3HT, RR-P3HT, and PCBM. The structure of RRa-P3HT is shown as an example of region-random structure of P3HT.

related to the mean free path of the photoelectron which is typically a few nanometers. UPS has been found to be very useful in determining the energy level alignment at organic interfaces.[21] Importantly, since different elements have characteristic sets of binding energies, XPS can be used to identify and determine the ratio of the elements present on the surface of a sample.[22] Besides, AR-XPS allows quantification of surface components as a function of film depth in the range of a few nanometers.

We also used optical absorption and photoluminescence (PL) spectroscopy, plus optical and PL microscopy, in order to better interpret the measured electronic energy levels and to build up energy and morphological models for the blend thin films with the UPS and XPS results. We show that ordering raises the HOMO level of P3HT (reducing its ionization potential) and that surface crystallization of RR-P3HT can occur under specific circumstances in RR-P3HT:PCBM blend films.

EXPERIMENTAL SECTION

Film Preparation. Regiorandom P3HT (RRa-P3HT) (regioregularity = 1:1 (head-to-head):(head-to-tail) linkages of regioisomers) was purchased from Aldrich. The weight-average molecular weight is ~87 kg/mol. Regioregular P3HT (RR-P3HT) was supplied by Merck Chemicals. The weight (M_w)- and number (M_n)-average molecular weights, polydispersity index and regioregularity are 54.2 kg/mol, 23.6 kg/mol, 2.29, and 94.2%, respectively. PCBM was purchased from API Service, Inc. All the materials were used as received. RRa-P3HT (RR-P3HT) solution was prepared by dissolving 12.5 mg of RRa-P3HT (RR-P3HT) in 1 mL of chlorobenzene and PCBM solution was prepared by dissolving 25 mg PCBM in 1 mL of chlorobenzene. The RRa-P3HT:PCBM solution was prepared by dissolving ~8.3 mg of RRa-P3HT with ~8.3 mg of PCBM in 1 mL of chlorobenzene solution. The RR-P3HT:PCBM solution was prepared by dissolving 10 mg of RR-P3HT with 10 mg of PCBM in 1 mL of chlorobenzene solution. For absorption measurements, films of ~50 nm thickness (as measured by an Alpha-step 200 automatic step profiler (Tencor Instruments)) were prepared by spin-coating solutions on glass substrates at 1500 rpm for 60 s. For other measurements, films of similar thickness were spin-coated (under comparable conditions) on top of poly(3,4-ethylenedioxythiophene) poly(styrenesulfonate) (PEDOT:PSS) films, themselves spin-coated on indium tin oxide (ITO) coated glass substrates to mimic the actual device configuration. For annealed films, the annealing condition is 140 °C for 30 min inside a nitrogen glovebox.

Optical Absorption and PL Measurements. Absorption spectra were recorded using a UV−vis spectrophotometer (UV-2550, Shimadzu). The PL spectra were obtained using a spectrofluorimeter (Fluorolog, Jobin Yvon Horiba) with excitation at 480 nm in air.

Optical Microscopy and PL Mapping. Optical images were taken with an optical microscope (Leica) with a 50x objective. PL mapping images were recorded under 633 nm excitation (50× objective) with a Renishaw inVia Raman microscope in a back scattering configuration. The excitation power is ~1 mW for RRa-P3HT:PCBM film and ~0.5 mW for RR-P3HT:PCBM film. The PL images were obtained by mapping the intensity at 2100 cm^{-1} (corresponding to ~730 nm).

UPS and AR-XPS Measurements. Ultraviolet and (angle-resolved) X-ray photoelectron spectroscopy measurements were performed with an Axis Ultra DLD system (Kratos Analytical Ltd.). For UPS measurements a He I lamp (energy ~21.22 eV) was used as the excitation source. The detection area was a spot of ~110 μm diameter. A bias of −18.49 V was applied to the sample, increasing the kinetic energy of the emitted photoelectrons to shift the observed spectrum away from 0 eV in order to observe features at low electron kinetic energy. From the onset of the secondary electron energy cutoff, E_{co}, we can calculate the work function, $\phi = h\nu - (E_{co} - E_F)$ where $h\nu$ is the excitation photon energy and E_F is the Fermi level. From the position of the low binding energy photoemission onset, E_{LBE} (the position where the two dashed lines intersect each other in (Figure 4a), the HOMO energy (E_{HOMO}) can be calculated with $E_{HOMO} = -(\phi + E_{LBE})$ with respect to the vacuum level. We performed several measurements (also for XPS and AR-XPS) on different regions of each film and confirmed that the results are similar. For XPS measurements, the base pressure in the analysis chamber of the system was 2×10^{-9} Torr. A monochromatic Al Kα (1486.6 eV) X-ray source operated at 15 kV and 10 mA emission was used for excitation. Survey scan spectra were collected over a binding energy range 1400 to −10 eV with 1 eV steps and a pass energy of 160 eV. A step size of 0.1 eV, pass energy 40 eV and appropriate energy ranges were chosen for high resolution narrow scans of selected elements. The detection area was ~700 μm × 300 μm. CasaXPS was used to quantify the spectra (survey scans) for the detectable elements. The integrated areas of the XPS peaks were calculated after correcting for the intensity calibration using the manufacturer's values determined for the instrument and subtracting linear backgrounds. Atomic ratios, C_i, were evaluated using the following equation:

$$C_i = \frac{I_i/S_i}{\sum_i I_i/S_i} \quad (1)$$

dx.doi.org/10.1021/ma102841e |*Macromolecules* 2011, 44, 2944–2952

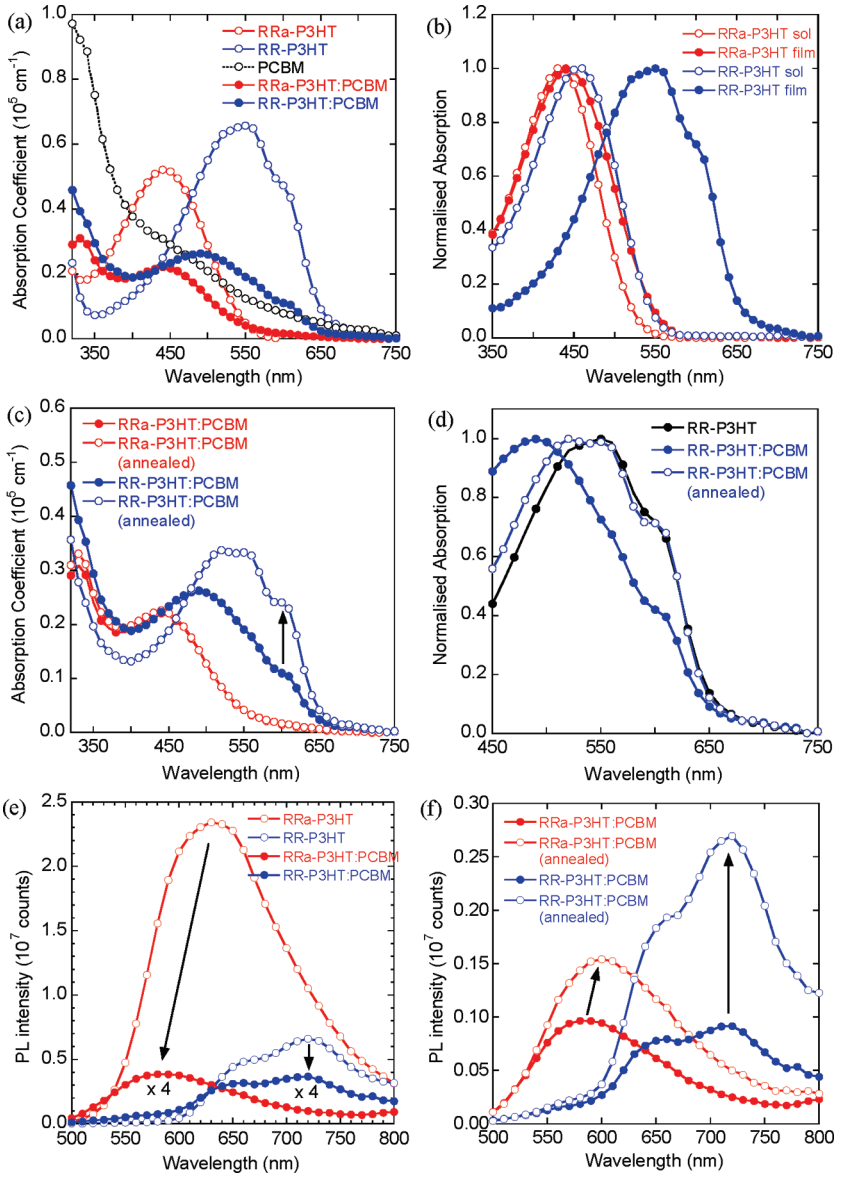

Figure 2. (a) Absorption spectra of RRa-P3HT, RR-P3HT, PCBM films and their blend films with PCBM. (b) Absorption spectra of RRa-P3HT, RR-P3HT films, RRa-P3HT (0.001 wt %), and RR-P3HT (0.001 wt %) in chlorobenzene solutions. Note that highly diluted solutions were used to ensure no aggregation of RR-P3HT molecules. (c) Absorption spectra of RRa-P3HT:PCBM and RR-P3HT:PCBM films before and after annealing. (d) Normalized absorption spectra of RR-P3HT and RR-P3HT:PCBM films before and after annealing. (e) PL spectra of RRa-P3HT, RR-P3HT films, and their blend films with PCBM (excited at 480 nm). The spectra of RRa-P3HT:PCBM and RR-P3HT:PCBM films are multiplied by a factor of 4 to make them more visible. Note that RR-P3HT films show the vibronic features at 670 and 720 nm. (f) PL spectra of RRa-P3HT:PCBM and RR-P3HT:PCBM films before and after annealing (excited at 480 nm).

where I is the peak area and S is the atomic sensitivity factor in the CasaXPS software. The S $2p_{3/2}$ and S $2p_{1/2}$ peaks are not resolved in the survey scans so the S 2p signal appears as a single peak. This is because the difference in binding energy of the two S 2p peaks is 1 eV, which is the same as the step size and less than the resolution of the spectrometer when operated at the settings used for the survey scans. Therefore, the calculated atomic ratio of S 2p includes both the S $2p_{3/2}$ and S $2p_{1/2}$ signals. The volume% of P3HT in the blend film is estimated by dividing the atomic ratio of P3HT in the blend film by the atomic ratio of pure P3HT film.

RESULTS AND DISCUSSION

Absorption and Photoluminescence. We first study the effects of ordering (crystallization) of P3HT polymers on the absorption and emission properties in thin films fabricated by on its own (homomaterials) and by blending with PCBM, and with additional thermal annealing (140 °C for 30 min inside a nitrogen glovebox). The chemical structures of regiorandom P3HT (RRa-P3HT), regioregular P3HT (RR-P3HT) and PCBM molecules are shown in Figure 1. X-ray diffraction measurement[23] has confirmed that RRa-P3HT film is amorphous and RR-P3HT film is semicrystalline.

The absorption spectra of ~50 nm thick films of homomaterials (RRa-P3HT, RR-P3HT, and PCBM) and their blends (RRa-P3HT:PCBM and RR-P3HT:PCBM) are shown in Figure 2a. The absorption spectrum of RR-P3HT film is significantly red-shifted compared to that of RRa-P3HT film, with a clearly distinguishable

shoulder located at ~600 nm (a spectral characteristics of crystalline P3HT).[24] The absorption coefficient (α) at the main peak of RR-P3HT film is larger than that of RRa-P3HT film (6.60 $\times$ 10^4 cm^{-1} at 550 nm vs 5.23 $\times$ 10^4 cm^{-1} at 440 nm respectively) indicating more densely packed P3HT polymer chains in crystalline phase. Using the absorption edge, we estimate the optical band gap (E_g) of these polymers in thin films, ~1.9 eV for RR-P3HT and ~2.2 eV for RRa-P3HT, showing that ordering (crystallization) of P3HT polymer chains decreases its optical band gap. Such a decrease in the optical band gap of P3HT due to the ordering of polymer chains is more obvious when we compare solutions to solid-state thin films (Figure 2b).

Upon the formation of solid state thin film, the semicrystalline RR-P3HT shows a dramatic red-shift in its main absorption peak (from 460 to 550 nm), but the amorphous RRa-P3HT shows only a little broadening of the absorption peak to longer wavelengths without significant shift of the main absorption peak (from 430 to 440 nm). Additional thermal annealing of these homomaterials in thin films does not induce any further ordering of the P3HT polymer chains, therefore no further changes were observed in the absorption spectra in terms of shape and intensity (data not shown).

On the other hands, by blending P3HT polymers with PCBM molecules, there is no measurable peak shift in the absorption spectrum for RRa-P3HT, but a significant blue-shift in the main absorption peak (from 550 to 490 nm) for RR-P3HT with much less absorption at ~600 nm ($I_{600\ nm}/I_{490\ nm}$ = 0.94 for RR-P3HT and 0.43 for RR-P3HT:PCBM blend, Figure 2, parts c and d). Upon annealing of this RR-P3HT:PCBM blend film, however, these changes are mostly recovered (i.e., a red-shift of the main absorption peak and an increase in the $I_{600\ nm}/I_{490\ nm}$ ratio to 0.82). These results indicate a disrupted ordering of P3HT polymer chains by addition of PCBM molecules in spin-coated RR-P3HT:PCBM blend thin films and a remarkable recovery of P3HT to its ordered phase due to annealing. There is no significant spectral changes in the absorption upon annealing RRa-P3HT:PCBM films.

The photoluminescence (PL) spectra of thin films of homomaterials (RRa-P3HT, RR-P3HT and PCBM) and their blends (RRa-P3HT:PCBM and RR-P3HT:PCBM) are shown in Figure 2e. The RRa-P3HT film has a broad PL spectrum peaking at 630 nm; on the other hand, the RR-P3HT film has a significantly red-shifted PL spectrum with distinguishable vibronic features peaking at 670 and 720 nm. More importantly, the PL intensity of RRa-P3HT film is 3.6 times stronger than that of RR-P3HT film. These observations are consistent with the characteristics of emission from different phases (amorphous vs crystalline) of P3HT molecules (i.e., red-shifted and less emissive PL from more ordered phase of the molecules).[24] By blending P3HT polymers with PCBM molecules, PL intensity is quenched; 24 times for RRa-P3HT:PCBM blend and 7.2 time for RR-P3HT:PCBM blend, respectively. Much more significant quenching of PL intensity in the RRa-P3HT:PCBM blend film can be attributed to much finer mixing of amorphous phase RRa-P3HT polymer chains with the PCBM molecules.[23] Compared to RRa-P3HT, the ordered phase of RR-P3HT chains seems to prevent PCBM molecules from being intimately mixed with the polymer chains, leading to less efficient interaction between them, so less quenching of P3HT emission. Different degrees of PL quenching in P3HT:PCBM blends observed here are consistent with reported values (50 times more quenching of RRa-P3HT emission in blend).[23]

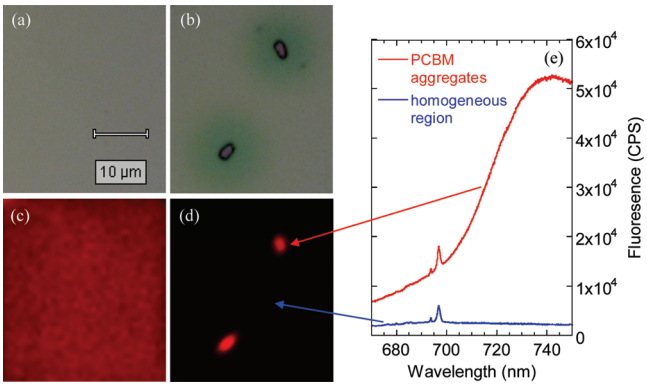

Figure 3. Optical images (a and b) and PL mapping images (c and d) for annealed RRa-P3HT:PCBM and RR-P3HT:PCBM films. PL images indicate emission intensities at 730 nm. (e) Emission spectra obtained in the homogeneous polymer-rich region and PCBM aggregate region of annealed RR-P3HT:PCBM film.

After annealing these blend films, there is an increase in the PL intensity; ~60% for RRa-P3HT:PCBM blend and ~200% for RR-P3HT:PCBM blend (Figure 2f). It is interesting to notice that for RRa-P3HT:PCBM blend, this increase in PL intensity is not correlated with the ground state absorption (no changes in absorption due to annealing), suggesting the origin of this increase in PL intensity to be mainly morphological. The PCBM molecules are diffused away from RRa-P3HT polymer chains during annealing, so that the interaction between RRa-P3HT polymer chains and PCBM molecules is reduced, leading to a recovery of emission from RRa-P3HT. The more substantial increase in PL intensity in RR-P3HT:PCBM blend after annealing might indicate much higher degree of phase separation between RR-P3HT polymer chains and PCBM molecules, which allows the formation of noticeably large PCBM aggregates (a few micrometers in size, Figure 3b).

Optical and PL Images. We study the thin film morphology of these two blend systems using optical microscopy and Raman spectroscopy. The optical images (a, b) and the PL images (c, d) of RRa-P3HT:PCBM and RR-P3HT:PCBM blend films after annealing are shown in Figure 3. The PL images reflect the local fluoresence intensity monitored at 730 nm (a peak of PCBM emission),[25] extracted from fluorescence background in the Raman spectra cross-mapped in the blend films with a micrometer spatial resolution under 633 nm excitation (See the Experimental section for more details).

There is a very homogeneous surface without any measurable features such as PCBM aggregates in the optical (Figure 3a) and PL (Figure 3c) images for the annealed RRa-P3HT:PCBM film. Contrary to this, the annealed RR-P3HT:PCBM film shows micrometer-sized domains in its optical image (Figure 3b). Atomic force microscope surface profiles reveal that these domains protrude ~400 nm from the surrounding homogeneous areas. The PL image clearly shows relatively low, but homogeneous (~1.1 times difference) fluorescence intensity across the annealed RRa-P3HT:PCBM film (Figure 3c) and very strong and highly fluorescent intensity mainly from the protruded domains in the annealed RR-P3HT:PCBM film (Figure 3d). The PL spectra obtained from the homogeneous region and the protruded domains in the annealed RR-P3HT:PCBM film are compared (Figure 3e), which show ~70 times stronger fluorescence signals from the protruded domains. This

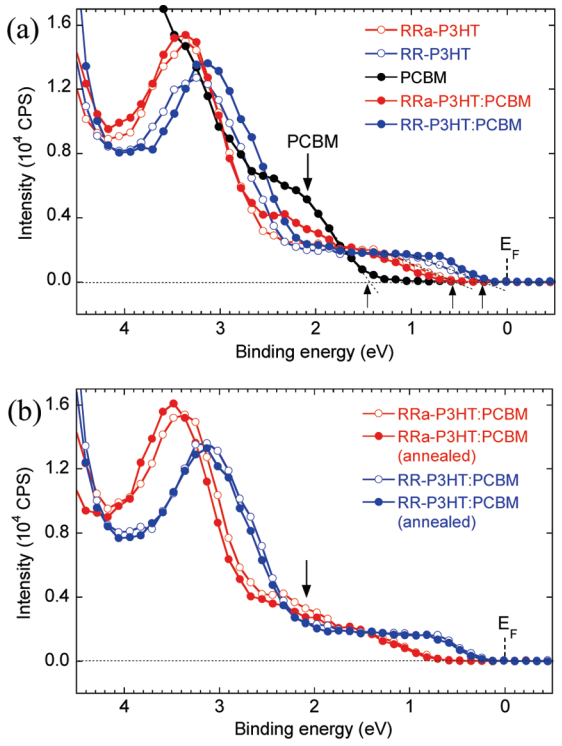

Figure 4. (a) UPS spectra of RRa-P3HT, RR-P3HT, PCBM films and their blend films. Intersection between the two dash lines in the figure is defined as the position of the low binding energy photoemission onset. The arrow indicates the PCBM component. (b) UPS spectra of RRa-P3HT:PCBM and RR-P3HT:PCBM films before and after annealing. The arrow indicates the PCBM component. The Fermi energy (E_F) is determined from the UPS spectrum of a clean silver sample.

data confirms that these protruded domains are PCBM-rich. Similar observation of fluorescence from PCBM aggregate in annealed RR-P3HT:PCBM film in Raman system has been reported.[25]

The total coverage of PCBM aggregates appears to be relatively small (only ~0.05% coverage of the total surface area) in this annealed RR-P3HT:PCBM blend film (~50 nm thick). Although the peak height of the domains is ~400 nm, it is still not sufficient to explain the significant increase in PL efficiency (~200%) measured after annealing, which is attributed to the phase separation between RR-P3HT polymer chains and PCBM molecules. Therefore, we consider that the PCBM aggregates are not only formed in the surface of the film, but also formed in the bulk of the film. We further notice that the PCBM aggregates in terms of amounts and sizes formed after annealing tend to depend strongly on the blend film thickness; i.e., the thicker the blend film is, the more and larger the PCBM aggregates are formed (for 50 nm (250 nm) film, area coverage ~0.05% (14.6%); size of PCBM aggregates can be ~3.6 μm × 1.5 μm (~20 μm × 4.2 μm).

UPS Measurements. We study the effects of ordering (crystallization) of P3HT polymers on the highest occupied molecular orbital (HOMO) energy levels in the thin films of homomaterials and blends with/without thermal annealing. Figure 4a shows UPS spectra measured in the thin films of homomaterials (RRa-P3HT, RR-P3HT, and PCBM) and their blends (RRa-P3HT:PCBM and RR-P3HT:PCBM) before annealing. The HOMO energy levels of these films are estimated from their measured UPS spectra by taking into account the Fermi-level as a binding energy reference. Note that the very low coverage (~0.05%) of PCBM aggregates at the film surface (or the film−air interface) in our 50-nm-thick annealed RR-P3HT:PCBM films facilitates the UPS signals measured within ~2−3 nm in depth (and also XPS in the next section) to be measured mainly in the homogeneous regions of these films, therefore not to be complicated by the roughness effect on these measurements. The HOMO energy levels (by UPS) and the chemical compositions (by XPS) reported in this paper are the average values based on the measurements in three different regions in each sample.

The energies of the HOMO levels of RRa-P3HT, RR-P3HT and PCBM films obtained from UPS spectra are −4.9, −4.6, and −5.8 eV respectively (within the experimental error of ±0.1 eV), showing that the HOMO level of RR-P3HT is ~0.3 eV higher lying than that of RRa-P3HT. We attribute this 0.3 eV reduction in the HOMO level of the P3HT film to the better ordering of polymer chains in regioregular P3HT (in which P3HT chains form a crystalline phase), compared to regiorandom P3HT (in which P3HT chains form an amorphous phase). By bringing polymer chains closer together (by $\pi-\pi$ stacking as for the case of RR-P3HT), the HOMO energy level of the polymer can be raised,[26] from which a relatively easier extraction of electrons can be expected. Such a regioregularity induced shift in the HOMO level (about hundreds of meV) of polythiophenes has been also measured in poly(3-alkylthiophenes) materials by cyclic voltammetry.[27] We consider, however, that the difference in polymer chain length between RR- and RRa-P3HT has little effect on this HOMO level shift as the average chain length of these two polymers (616 and 989 thiophene units for RR-P3HT and RRa-P3HT, respectively, estimated from their M_w values) are well above the effective conjugation length of polythiophene (~10 thiophene units).[28] We note that the HOMO energy levels of RR-P3HT and PCBM films obtained from our UPS spectra are in good agreement with the previously reported values of −4.6 and −5.96 eV, respectively.[29−31]

After annealing these thin films of homomaterials, we measured similar HOMO energy levels for RRa-P3HT, RR-P3HT and PCBM films (not shown). This implies, in particular for RR-P3HT film, that the ordering of P3HT polymer chains occurs mainly during spin-coating process, already forming a semicrystalline phase of P3HT molecules in the spin-coated film, and there is no further significant ordering upon annealing of this film.

For the blend thin films, when RRa-P3HT was blended with PCBM, the shape of the UPS spectrum of the blend becomes the superposition of each of RRa-P3HT and PCBM films (Figure 4a), indicating that there is a considerable amount of PCBM within the measured topmost surface layer (~2−3 nm), as most of the detected signals in UPS measurement comes from this thin layer. The RRa-P3HT HOMO level in the blend film is ~0.08 eV lower lying than that of pure RRa-P3HT film, which is within the experimental error of ±0.1 eV. On the other hand, for the RR-P3HT:PCBM blend film, the shape of the UPS spectrum is very similar to that of pure RR-P3HT film without any obvious contribution from PCBM, suggesting that the topmost layer in this blend film contains mainly RR-P3HT.

The UPS spectra of the blend films before and after annealing are shown in Figure 4b. After annealing the RRa-P3HT:PCBM blend film, we notice that the UPS signal from PCBM is slightly reduced, implying that some PCBM molecules may diffuse away from this topmost layer. For the RR-P3HT:PCBM blend film, there are no measurable changes in the UPS spectra before and after annealing. Based on our observations that the ordering of RR-P3HT molecules raises the HOMO energy level upward and that the HOMO energy level of RR-P3HT in the blend films

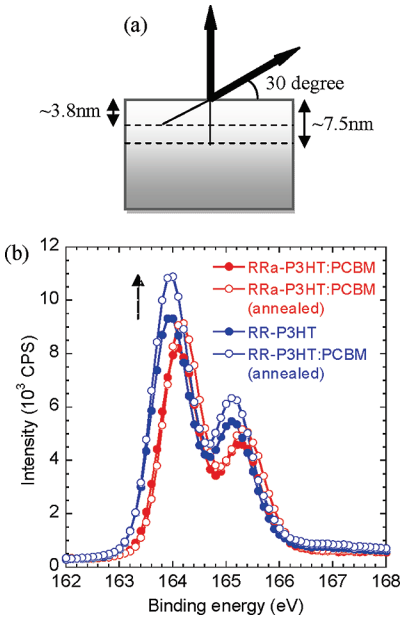

Figure 5. (a) Experimental geometry for the (angle resolved) − X-ray photoelectron spectroscopic measurements. Take off angle of photoelectron is defined as the angle between sample surface and the detector. At 90° (30°), most signal is collected within the topmost ~7.5 nm (~ 3.8) layer. (b) S 2p (S $2p_{3/2}$ and S $2p_{1/2}$) core-level XPS spectra of RRa-P3HT:PCBM and RR-P3HT:PCBM films before and after annealing at takeoff angle of 90°.

(for both pristine and annealed) is similar to that of pure RR-P3HT films (for both pristine and annealed), we suggest that the RR-P3HT polymer chains at the topmost layer of all these films have a similar degree of molecular order (crystallization).

Contrary to the UPS measurements, much less ordering of RR-P3HT molecules in the pristine RR-P3HT:PCBM blend film is measured compared to the pure RR-P3HT film and the annealed blend film by the absorption spectroscopy, as indicated by the relatively weak absorption shoulder at 600 nm in Figure 2d. Since the absorption spectroscopy probes the order of P3HT molecules through the whole bulk of the film (~50 nm thick), differently from the UPS measurement which is sensitive only to the topmost layer (~2−3 nm thick) of the film, we suggest different degrees of order of P3HT molecules occur even within a film; i.e., for the pristine RR-P3HT:PCBM blend film, the RR-P3HT molecules are relatively more ordered (crystallized) at the topmost layer of the film than in the bulk. We consider this observation as a "surface enhanced crystallization" of RR-P3HT in this pristine RR-P3HT:PCBM blend thin film. Such an enhanced crystallization of RR-P3HT molecules at the topmost surface may be responsible for the RR-P3HT-rich top layer generally observed in the RR-P3HT:PCBM blend films prepared on PEDOT:PSS coated substrates.[6,13,15] We note that such surface crystallization has been observed for other polymers.[32] We investigate further this RR-P3HT crystallization at the top surface of the blend films using AR-XPS in the next section.

XPS Measurements. Figure 5 shows the S 2p core-level XPS spectra at a takeoff angle of 90° for the RRa-P3HT:PCBM and RR-P3HT:PCBM blend films before and after annealing. The takeoff angle of the photoelectron represents the angle between the sample surface and the detector, such that at 90°, the photoemission signal will mostly be collected from the top surface of ~7.5 nm in depth (photoelectron escape depth ~2.5 nm for S 2p) (Figure 5a).[33] The S 2p signal arises solely from the P3HT and is a distinct marker for that polymer. The S 2p signal is split by spin−orbit coupling into S $2p_{3/2}$ and S $2p_{1/2}$ components in a 1:1.7−1.8 ratio separated by 1.1−1.2 eV. For both pristine and annealed blend films, the observed binding energy of S $2p_{3/2}$ peak of the RR-P3HT:PCBM blend films (164.0 eV) are ~0.1−0.2 eV smaller than that of the RRa-P3HT:PCBM blend films (164.1−164.2 eV). There is stronger S 2p signal from the RR-P3HT:PCBM blend films than from the RRa-P3HT:PCBM blend films suggesting that in their respective blend films, there are more RR-P3HT polymers on the film surface than RRa-P3HT. After annealing, the S 2p signals for both blend films increase reflecting the larger amount of both RR-P3HT and RRa-P3HT polymers on the surface of the blend films.

The atomic ratios of the carbon, oxygen and sulfur atoms near the surface of the pristine and annealed RRa-P3HT:PCBM and RR-P3HT:PCBM blend films are summarized in Table 1. For the pristine films, we find that the atomic ratio of sulfur is similar for RR-P3HT (9.3%) and RRa-P3HT (9.5%) and atomic ratio of carbon (94.4%) and oxygen (5.6%) of PCBM is higher than that of the P3HT (carbon 89.0% and oxygen 1.6%), consistent with their chemical structures. Note that carbon and oxygen are common contaminants and therefore the estimation of their atomic ratios is only for comparison purpose.

There is relatively more amount of RRa-P3HT (5.4 at. % S, 58 vol. % RRa-P3HT) within the ~7.5 nm thick top layer for the pristine RRa-P3HT:PCBM film. This can be explained by the lower surface energy of P3HT (26.9 mN/m) than that of PCBM (38.2 mN/m),[34] so P3HT is preferentially favorable to cover the film−air interface to reduce the overall surface energy.[35] Interestingly, there is an even larger amount of RR-P3HT (7.3 at. % S, 78 vol. % RR-P3HT) on the surface of nonannealed RR-P3HT:PCBM film, consistent with recent reports.[6,13] To probe the phase-separated thin film structure even closer to the topmost layer, we also performed XPS measurements at takeoff angle of 30° (most sensitive to the ~3.8 nm topmost layer) (Figure 5a). We find that for both RRa-P3HT:PCBM and RR-P3HT:PCBM films even more polymers are accumulated on this topmost surface, i.e. 68 vol. % (6.3 at. % S) for RRa-P3HT and 92 vol. % (8.6 at. % S) for RR-P3HT, respectively. It shows the nearly pure RR-P3HT topmost layer in RR-P3HT:PCBM films. It has been recently reported that a nearly pure P3HT layer was formed on the surface of RR-P3HT:PCBM films deposited on PEDOT:PSS-coated or silicon substrates monitored by neutron scattering technique.[15]

The surface energies of RRa-P3HT and RR-P3HT are expected to be similar as they have the similar chemical structures. Therefore, the difference in the amount of P3HT molecules on the topmost surface can be mainly attributed to the better ordering nature of RR-P3HT molecules (better crystallization than RRa-P3HT). The ordering of RR-P3HT molecules may phase separate the PCBM molecules away from the surface. This agrees well with our UPS results, which show that there is considerably less PCBM (or more RR-P3HT) on the surface of nonannealed RR-P3HT:PCBM film. A similar observation of surface crystallization of poly(9,9-dioctylfluorene) (PFO) has been reported when it is blended with poly(9,9-dioctylfluorene-*alt*-benzothiadiazole) (F8BT) in thin films.[36] The origin of this PFO-rich layer is assigned to the crystallization nature of PFO polymer on the surface of the film, which further phase separates the F8BT away from the surface.

When the RRa-P3HT:PCBM film is annealed, both the ~3.8 nm topmost and the ~7.5 nm top layers show an increase in RRa-P3HT content, suggesting that some PCBM molecules

Table 1. Atomic Ratio of the Elements and Volume Ratio of P3HT in Non-Annealed RRa-P3HT:PCBM Film, Non-Annealed RR-P3HT:PCBM Film, and Their Annealed Films (also Shown for Pristine RRa-P3HT, RR-P3HT, and PCBM Films)

	probing depth from the top surface (nm)[a]	C (%)[b]	O (%)[b]	S (%)	relative volume of P3HT (%)[c]
RRa-P3HT	-	89	1.5	9.5	-
RR-P3HT	-	89	1.7	9.3	-
PCBM	-	94.4	5.6	-	-
RRa-P3HT:PCBM	~7.5	92.3 ± 0.2	2.3 ± 0.2	5.4 ± 0.0	58 ± 1
	~3.8	91.6 ± 0.2	2.1 ± 0.2	6.3 ± 0.1	68 ± 2
RR-P3HT:PCBM	~7.5	91.0 ± 0.1	1.7 ± 0.0	7.3 ± 0.1	78 ± 3
	~3.8	89.7 ± 0.1	1.7 ± 0.1	8.6 ± 0.0	92 ± 2
annealed	~7.5	92.1 ± 0.1	1.8 ± 0.0	6.1 ± 0.1	66 ± 2
RRa-P3HT:PCBM	~3.8	91.7 ± 0.2	1.6 ± 0.2	6.7 ± 0.1	72 ± 3
annealed	~7.5	90.6 ± 0.1	1.3 ± 0.0	8.1 ± 0.1	87 ± 3
RR-P3HT:PCBM	~3.8	90.0 ± 0.1	1.2 ± 0.2	8.8 ± 0.2	95 ± 4

[a] Based on the photoelectron signal of S 2p. [b] The binding energies of C 1s and O 1s are ~285.05 ± 0.1 eV and ~533.4 ± 0.4 eV, respectively. [c] The relative volume of P3HT (%) is the volume fraction of P3HT at the top layer of the blend films compared to a pure P3HT top layer. The error bars quoted here are determined from various values obtained from three different areas on each sample.

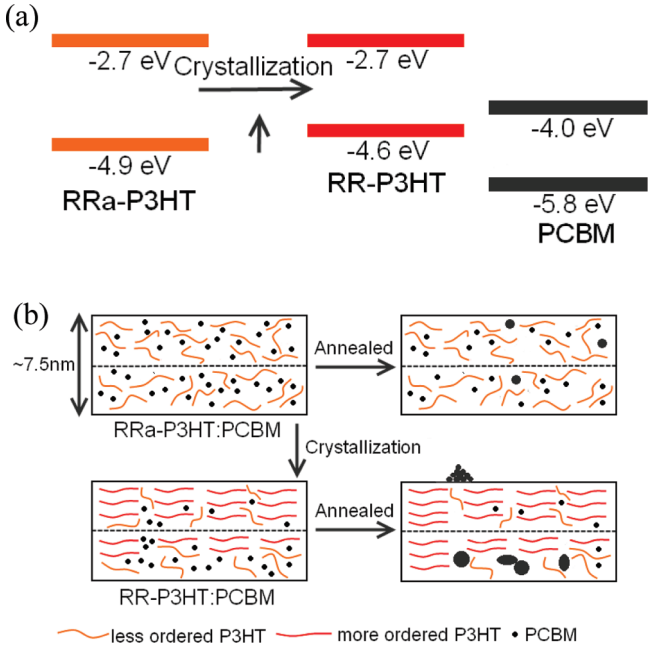

Figure 6. (a) Simplified HOMO and LUMO energy levels of RRa-P3HT, RR-P3HT and PCBM films and (b) morphological models of RRa-P3HT:PCBM, RR-P3HT:PCBM films before and after thermal annealing.

may diffuse away from these layers. This is consistent with our UPS data, which show that after annealing the RRa-P3HT:PCBM film, there is less PCBM contribution to the UPS spectrum. This is probably due to the fact that thermal annealing provides an additional driving force for phase-separation to occur between P3HT and PCBM molecules and to reach more thermodynamically stable thin film morphology in the blend.[13,35] When the RR-P3HT:PCBM film is annealed, the ~7.5 nm top layer also shows an increase in RR-P3HT content. However, for the ~3.8 nm topmost layer, the RR-P3HT content in the annealed blend film (~95 ± 4%) is very similar to that in nonannealed blend film (~92 ± 2%). This suggests that the topmost layer is composed of already highly crystallized P3HT molecules even in nonannealed state, consistent with surface enhanced crystallization of P3HT and no changes observed in the HOMO energy levels before and after annealing. Note that even within the ~7.5 nm top layer, there is a different degree of crystallization with the highest crystallization of P3HT on the topmost layer.

Energy Levels and Thin Film Morphology. Based on absorption, PL, optical microscopy, UPS, and AR-XPS results observed in previous sections, we discuss the frontier energy levels (HOMO and LUMO) and propose morphological models of the blend films before and after annealing.

Figure 6a shows the HOMO and LUMO energy levels for RRa-P3HT, RR-P3HT, and PCBM films. The LUMO level is estimated by simply adding the optical band gap E_g (estimated from absorption spectra) of the material to the HOMO level. It shows that ordering P3HT chains raises the HOMO level by ~0.3 eV with no significant changes in the LUMO level, indicating that crystallization makes P3HT molecules more susceptible to oxidation. This reduced HOMO level may also affect the V_{oc} value in P3HT based photovoltaic (PV) devices. We note that a ~0.25 V increase in the V_{oc} value has been observed in PV devices showing ~0.87 V for RRa-P3HT:PCBM and ~0.62 V for RR-P3HT:PCBM,[37] consistent with our observation.

Our proposed (surface) morphological models for the blend thin films before and after annealing are shown in Figure 6b. For nonannealed RRa-P3HT:PCBM film, there are relatively more RRa-P3HT polymers in the ~7.5 nm top layer (~58%) and RRa-P3HT polymers and PCBM molecules are well mixed within this top layer. It is evident by measured strong PL quenching in this blend film that such good mixing occurs also in the bulk of the blend film. For the nonannealed RR-P3HT:PCBM film, there are significantly more RR-P3HT polymers in the top layer (~78%) with the almost pure P3HT topmost layer (~ 92%). These P3HT dominated top and topmost layers may create unfavorable vertical thin film structure for a conventional RR-P3HT:PCBM devices, i.e., hole transporting P3HT polymers next to electron-collecting electrode.

After thermal annealing of the RRa-P3HT:PCBM film, some PCBM molecules diffuse away from the top surface leading an increase in RRa-P3HT content (~ 66%). The increase in PL quantum yield after annealing of this film tends to indicate that some PCBM aggregates are formed after annealing. For the annealed RR-P3HT:PCBM film, there is no further changes of the amount of

P3HT polymers within the ~3.8 nm topmost layer, but the underneath layer (~3.8−7.5 nm below the film surface), which is not initially highly crystallized before annealing, is now further crystallized, resulting in the accumulation of larger amount of P3HT polymers within this layer (~78% to ~87%) and the formation of distinctive micrometer-sized PCBM aggregates. Based on the much stronger increase in PL quantum yield after annealing of RR-P3HT:PCBM film, we consider that there are more and larger PCBM aggregates (also in the bulk film) in this blend film than RRa-P3HT:PCBM film. The micrometer-sized PCBM aggregates as observed from optical images on the surface of RR-P3HT:PCBM film (although very few %) could have been generated by diffusion of PCBM molecules from the underneath layer.

It is important to consider different characteristics of the disordered phase of P3HT compared to its ordered phase. Since the disordered phase of P3HT shows the lower-lying (higher) HOMO level and better mixing with PCBM molecules, it would be interesting to make use of these characteristics to optimize the performance of P3HT:PCBM devices, for example, creating the active layer with crystallized P3HT (RR-P3HT) embedded in the amorphous P3HT (RRa-P3HT) matrix. By doing so, one can control to a certain degree the V_{oc} (via HOMO levels) and J_{sc} (via better mixing) values. We notice that it has been suggested that for an average molecular weight (30−70 kg/mol) of RR-P3HT, a rather high polydispersity (>2) is generally required to produce a good power conversion efficiency for RR-P3HT:PCBM solar cells.[38,39] As P3HT crystallization depends on the polymer chain length, this high polydispersity might lead to the formation of different amounts of ordered and disordered phases of P3HT. We note that the discussion above is based on measurements performed in thin films and annealing steps taken before a top electrode evaporated. Further work is in progress to clarify any effects induced by post annealing of the blend films performed after evaporating the top electrode for a complete device. Our initial study shows that the size of the PCBM aggregates when annealed with cathode on top of the film is significantly reduced.

CONCLUSIONS

We observed that ordering the P3HT chains raises the HOMO energy level of P3HT thin films (reducing ionization potential) and that this ordering of P3HT occurs preferentially at the film−air interface in RR-P3HT:PCBM thin films (spin-coated on ITO/PEDOT:PSS substrates). This crystallization induces phase separation between P3HT and PCBM molecules, pushing PCBM molecules further away from the film−air interface, leading to an undesirable vertical structure with a nearly pure P3HT layer (hole transport layer) at the film−air interface (where an electron collecting electrode is usually deposited on for a conventional photovoltaic device architecture). Even within the ~7.5 nm top layer from the film−air interface, there exists a different degree of crystallization of RR-P3HT molecules with more significantly crystallized P3HT molecules on the topmost layer (~3.8 nm thick). We note that the disordered phase of P3HT has deeper HOMO level and better mixing with PCBM, which may play an important role in controlling thin film structure of P3HT:PCBM blends and thus corresponding device performance.

AUTHOR INFORMATION

Corresponding Author

*E-mail: (J.-S/K.) ji-seon.kim@imperial.ac.uk; (C.E.M.) craig.murphy@npl.co.uk.

ACKNOWLEDGMENT

This work is funded by an EPSRC-NPL Post-Doctoral Research Partnership (EP/G062056/1) and by BIS National Measurement System IRD C02 Plastic Electronics project grant (2008). JSK thanks the World Class University (WCU) Project in Korea (Grant No. *R*32-10051).

REFERENCES

(1) Gunes, S.; Neugebauer, H.; Sariciftci, N. S. *Chem. Rev.* **2007**, *107*, 1324–1338.
(2) Mayer, A. C.; Scully, S. R.; Hardin, B. E.; Rowell, M. W.; McGehee, M. D. *Mater. Today* **2007**, *10*, 28–33.
(3) Bredas, J.-L.; Norton, J. E.; Cornil, J.; Coropceanu, V. *Acc. Chem. Res.* **2009**, *42*, 1691–1699.
(4) Ma, W. L.; Yang, C. Y.; Gong, X.; Lee, K.; Heeger, A. J. *Adv. Funct. Mater.* **2005**, *15*, 1617–1622.
(5) Kim, Y.; Cook, S.; Tuladhar, S. M.; Choulis, S. A.; Nelson, J.; Durrant, J. R.; Bradley, D. D. C.; Giles, M.; McCulloch, I.; Ha, C. S.; Ree, M. *Nat. Mater.* **2006**, *5*, 197–203.
(6) Campoy-Quiles, M.; Ferenczi, T.; Agostinelli, T.; Etchegoin, P. G.; Kim, Y.; Anthopoulos, T. D.; Stavrinou, P. N.; Bradley, D. D. C.; Nelson, J. *Nat. Mater.* **2008**, *7*, 158–164.
(7) Li, G.; Shrotriya, V.; Huang, J. S.; Yao, Y.; Moriarty, T.; Emery, K.; Yang, Y. *Nat. Mater.* **2005**, *4*, 864–868.
(8) Chiu, M.-Y.; Jeng, U.-S.; Su, C.-H.; Liang, K. S.; Wei, K.-H. *Adv. Mater.* **2008**, *20*, 2573–2578.
(9) Mihailetchi, V. D.; Xie, H.; De Boer, B.; Koster, L. J. A.; Blom, P. W. M. *Adv. Funct. Mater.* **2006**, *16*, 699–708.
(10) Yang, X.; Loos, J. *Macromolecules* **2007**, *40*, 1353–1362.
(11) Keivanidis, P. E.; Clarke, T. M.; Lilliu, S; Agostinelli, T.; Emyr Macdonald, J.; Durrant, J. R.; Bradley, D. D. C.; Nelson, J. *J. Phys. Chem. Lett.* **2010**, *1*, 734–738.
(12) Veldman, D.; Ipek, O.; Meskers, S. C. J.; Sweelssen, J.; Koetse, M. M.; Veenstra, S. C.; Kroon, J. M.; van Bavel, S. S.; Loos, J.; Janssen, R. A. J. *J. Am. Chem. Soc.* **2008**, *130*, 7721–7735.
(13) Xu, Z.; Chen, L.-M.; Yang, G.; Huang, C.-H.; Hou, J.; Wu, Y.; Li, G.; Hsu, C.-S.; Yang, Y. *Adv. Funct. Mater.* **2009**, *19*, 1227–1234.
(14) Germack, D. S.; Chan, C. K.; Hamadani, B. H.; Richter, L. J.; Fischer, D. A.; Gundlach, D. J.; DeLongchamp, D. M. *Appl. Phys. Lett.* **2009**, *94*, 233303.
(15) Kiel, J. W.; Kirby, B. J.; Majkrzak, C. F.; Maranville, B. B.; Mackay, M. E. *Soft Matter* **2010**, *6*, 641–646.
(16) Parnell, A. J.; Dunbar, A. D. F.; Pearson, A. J.; Staniec, P. A.; Dennison, A. J. C.; Hamamatsu, H.; Skoda, M. W. A.; Lidzey, D. G.; Jones, R. A. L. *Adv. Mater.* **2010**, *22*, 2444–2447.
(17) Felicissimo, M. P.; Jarzab, D.; Gorgoi, M.; Forster, M.; Scherf, U.; Scharber, M. C.; Svensson, S.; Rudolf, P.; Loi, M. A. *J. Mater. Chem.* **2009**, *19*, 4899–4901.
(18) Moon, J. S.; Lee, J. K.; Cho, S.; Byun, J.; Heeger, A. J. *Nano Lett.* **2009**, *9*, 230–234.
(19) Van Bavel, S. S.; Sourty, E.; De With, G.; Loos, J. *Nano Lett.* **2009**, *9*, 507–513.
(20) Scharber, M. C.; Muhlbacher, D.; Koppe, M.; Denk, P.; Waldauf, C.; Heeger, A. J.; Brabec, C. J. *Adv. Mater.* **2006**, *18*, 789–794.
(21) Braun, S.; Salaneck, W. R.; Fahlman, M. *Adv. Mater.* **2009**, *21*, 1450–1472.
(22) Kim, J. S.; Ho, P. K. H.; Murphy, C. E.; Friend, R. H. *Macromolecules* **2004**, *37*, 2861–2871.
(23) Campoy-Quiles, M.; Kanai, Y.; El-Basaty, A.; Sakai, H.; Murata, H. *Org. Electron.* **2009**, *10*, 1120–1132.
(24) Korovyanko, O. J.; Osterbacka, R.; Jiang, X. M.; Vardeny, Z. V. *Phys. Rev. B* **2001**, *64*, 235122.
(25) Wang, X.; Zhang, D.; Braun, K.; Egelhaaf, H.-J.; Brabec, C. J.; Meixner, A. J. *Adv. Funct. Mater.* **2010**, *20*, 492–499.
(26) Beljonne, D.; Cornil, J.; Sirringhaus, H.; Brown, P. J.; Shkunov, M.; Friend, R. H.; Bredas, J.-L. *Adv. Funct. Mater.* **2001**, *11*, 229–234.

(27) Skompska, M. M.; Szkurlat, A. *Electrochim. Acta* **2001**, *46*, 4007–4015.
(28) Gierschner, J.; Mack, H. G.; Egelhaaf, H. J.; Schweizer, S.; Doser, B.; Oelkrug, D. *Synth. Met.* **2003**, *138*, 311–315.
(29) Osikowicz, W.; De Jong, M. P.; Salaneck, W. R. *Adv. Mater.* **2007**, *19*, 4213–4217.
(30) Zhang, F. J.; Vollmer, A.; Zhang, J.; Xu, Z.; Rabe, J. P.; Koch, N. *Org. Electron.* **2007**, *8*, 606–614.
(31) Akaike, K.; Kanai, K.; Yoshida, H.; Tsutsumi, J.; Nishi, T.; Sato, N.; Ouchi, Y.; Seki, K. *J. Appl. Phys.* **2008**, *104*, 023710.
(32) Factor, B. J.; Russell, T. P.; Toney, M. F. *Phys. Rev. Lett.* **1991**, *66*, 1181–1184.
(33) Yim, K.-H.; Doherty, W. J.; Salaneck, W. R.; Murphy, C. E.; Friend, R. H.; Kim, J. S. *Nano Lett.* **2010**, *10*, 385–392.
(34) Wang, X.; Ederth, T.; Inganas, O. *Langmuir* **2006**, *22*, 9287–9294.
(35) Bjorstrom, C. M.; Bernasik, A.; Rysz, J.; Budkowski, A.; Nilsson, S.; Svensson, M.; Andersson, M. R.; Magnusson, K. O.; Moons, E. *J. Phys.: Condens. Matter* **2005**, *17*, L529–L534.
(36) Chappell, J.; Lidzey, D. G.; Jukes, P. C.; Higgins, A. M.; Thompson, R. L.; O'Connor, S.; Grizzi, I.; Fletcher, R.; O'Brien, J.; Geoghegan, M.; Jones, R. A. L. *Nat. Mater.* **2003**, *2*, 616–621.
(37) Vandewal, K.; Gadisa, A.; Oosterbaan, W. D.; Bertho, S.; Banishoeib, F.; Van Severen, I.; Lutsen, L.; Cleij, T. J.; Vanderzande, D.; Manca, J. V. *Adv. Funct. Mater.* **2008**, *18*, 2064–2070.
(38) Dennler, G.; Scharber, M. C.; Brabec, C. J. *Adv. Mater.* **2009**, *21*, 1323–1338.
(39) Ma, W.; Kim, J. Y.; Lee, K.; Heeger, A. J. *Macromol. Rapid Commun.* **2007**, *28*, 1776–1780.